In situ measurements of viscoelastic properties of biomass during hydrothermal treatment to assess the kinetics of chemical alterations

Julia Parlatore Lancha, Julien Colin, Giana Almeida, Patrick Perre

In situ measurements of viscoelastic properties of biomass during hydrothermal treatment to assess the kinetics of chemical alterations

Julia Parlatore Lancha*[1], Julien Colin[1,2], Giana Almeida[3], Patrick Perré[1,2]

[1] Université Paris-Saclay, CentraleSupélec, Laboratoire de Génie des Procédés et Matériaux, SFR Condorcet FR CNRS 3417, Centre Européen de Biotechnologie et de Bioéconomie (CEBB), 51110 Pomacle, France

[2] Université Paris-Saclay, CentraleSupélec, Laboratoire de Génie des Procédés et Matériaux, 8-10 rue Joliot-Curie, 91190 Gif-sur-Yvette, France

[3] Université Paris-Saclay, INRAE, AgroParisTech, UMR SayFood, 91300 Massy, France

*Corresponding author: julia.parlatore-lancha@centralesupelec.fr

Abstract

This work aimed to use continuous measurements of viscoelastic properties to evaluate the effect of hydrothermal treatment on poplar samples. Different conditions (temperature and pre-soaking liquid: acidic, neutral and alkaline) were tested on wood in both tangential and radial directions. Two viscoelastic properties were determined: the modulus of elasticity and the stress relaxation. The applicability of these properties as indicators of the kinetics of biomass deconstruction was also evaluated, thanks to the chemical analyses performed on the treated solid and the recovered liquid phase. The ultimate goal is to build a macroscopic indicator capable of establishing rules to optimize the hydrothermal treatment before the explosion stage. The joint use of the two parameters succeeded in revealing the effects of chemical degradation, including the coexistence of cleavage and re-condensation and the impact of process conditions (temperature, residence time, and pre-soaking liquid). The monotonous behavior of stress relaxation is a major asset as a possible macroscopic indicator of biomass deconstruction.

Keywords: Acidic, Alkaline, Lignocellulosic biomass, Steam explosion; Modulus of elasticity; Viscoelasticity; Poplar

1. Introduction

Lignocellulosic biomass constitutes one of the most abundant renewable sources of carbon (Sun et al., 2015). It has received increased attention in recent years as an alternative feedstock for industries such as biofuel and bio-based chemical production. However, as a result of evolution, lignocellulosic components—and especially wood—play the role of mechanical support in plants and help them withstand biological degradation. This natural recalcitrance, therefore, presents a significant challenge for industrialization. Regardless of the application, a pretreatment step is necessary to promote subsequent enzymatic hydrolysis by increasing the accessibility of polysaccharides (Ewanick and Bura, 2010).

Several pretreatment methods have been proposed. Among them, steam explosion seems to be best suited to meet industrial needs, for example, the efficient treatment of a wide variety of biomass sources (Haghighi Mood et al., 2013; Limayem and Ricke, 2012). It involves a hydrothermal step—during which biomass is subjected to high temperature under saturated steam conditions—followed by explosive decompression. Ideally, hydrothermal treatment should promote the separation of the three main components of lignocellulosic biomass (cellulose, hemicellulose, and lignin) with limited changes to their molecular structures. An increase in the porosity, as well as the reduction of cellulose crystallinity, are also expected for enhanced accessibility. At the same time, an ideal pretreatment should limit the formation of sugar degradation products (such as furfural and 5-hydroxymethylfurfural) and other inhibitory compounds (Nitsos et al., 2013).

The chemical degradation mechanisms occurring during hydrothermal treatment, especially those involving the hydrolysis of polysaccharides, are well documented in the literature. Under high temperatures, water autoionizes and forms hydronium ions that act as catalyzers for a series of hydrolysis reactions (Garrote et al., 1999). Hemicelluloses are the most susceptible components of the cell wall to this kind of reaction, probably due to their amorphous structure (Asada et al., 2015; Lancha et al., 2020; Liu et al., 2012). The first hydrolysis reaction is a split of the acetyl side groups, resulting in the production of acetic acid. The formation of this organic acid has a catalyzing effect and promotes the hydrolysis of hemicelluloses into oligo- and monosaccharides (Asada et al., 2015; Garrote et al., 1999). To a lesser extent, lignin is also affected by hydrolysis. Cleavage of β-O-4' aryl ether linkages has been observed to a significant extent even at 150 °C, due to their low thermal stability (Li et al., 2007; Samuel et al., 2013). Poplar can be particularly affected by this mechanism, as its lignins are predominantly composed of β-O-4' bonds (Barros et al., 2015; Lapierre, 1993; Lapierre et al., 1995; Mansfield et al., 2012). Lignin depolymerization is, however, often accompanied by condensation reactions. The cleavage of the most thermolabile linkages (β-O-4') gives rise to a rearranged lignin structure, rich in resistant bonds, such as β-β', β-5', and 5-5' (Assor et al., 2009; Auxenfans et al., 2017; Obame et al., 2019; Xiao et al., 2014). Additionally, polysaccharide degradation products are also susceptible to polymerization and condensation reactions, forming aromatic lignin-like structures (Shinde et al., 2018).

The pretreatment conditions greatly affect the outcomes of the entire production chain and, thus, must be optimized. Depending on the planned application and the desired physico-chemical characteristics, acidic or alkaline pre-soaking media can also be deployed (Chadni et al., 2019; Obame et al., 2019). Diluted sulfuric acid has been widely used in biomass pretreatment to increase sugar yields (Trajano and Wyman, 2013; Waldron, 2010). Alkaline

pretreatments, on the other hand, enhance lignin solubilization and require milder treatment conditions, limiting the formation of inhibitory products (Jönsson and Martín, 2016; Kim et al., 2016).

Mechanical tests can be used to assess the properties of a material. Young's modulus, for example, has long been used as a measure of polymer degradation (Dwianto et al., 1999; Wypych, 2016). More specifically, previous works have proven that viscoelastic properties are good indicators of biomass degradation during hydrothermal treatment (Assor et al., 2009; Mokdad et al., 2018), reflecting structural rearrangements of the cell wall components as well as changes in their molecular and supramolecular structure. In this case, the evolution of creep in time is likely to be due to the additive effects of treatment duration that alters the macromolecular structure and the effect of time on the viscoelastic behavior (Passard and Perré, 2005). To address this confusion, cyclic protocols, such as harmonic tests, are needed to decouple the effects of treatment duration with the effect of time on the viscoelastic creep (Placet et al., 2008, 2007).

The present work aims to use in-line measurements during hydrothermal treatment to assess the effects of operating conditions (temperature, pre-soaking liquid) on viscoelastic properties. For this purpose, poplar (*Populus euro-americana* 'Koster') tested across the grain was used as a biomass model. Two viscoelastic properties, tested under uniaxial compression, were measured: the apparent modulus of elasticity and the stress relaxation. Performing rheological tests under the severe conditions imposed by hydrothermal treatments (high temperature and saturated steam) was possible because of an original device conceived and built by our team (Mokdad et al., 2018). The pertinence of these properties as indicators of biomass deconstruction was assessed, with the ultimate goal of

finding a macroscopic indicator likely to provide guidelines to optimize the hydrothermal treatment prior to the explosion step.

2. Material and methods

2.1. Poplar samples

The samples were collected from a 25-year-old poplar tree (*Populus euro-americana* 'Koster') cultivated in Auménancourt-le-Petit (Marne, northeastern France). Green logs were cut in boards that were subsequently dried and stored before sample preparation. A defect-free board was selected, from which 8 x 8 x 8 mm^3 (radial - R, tangential - T, longitudinal - L) cubes were cut. To minimize the natural variability of wood, all samples were taken from the same straight line parallel to the longitudinal direction.

For chemical analysis, both native and treated samples were ground. Their moisture content was measured on a fraction of the powder and then the mass used for the analysis was corrected to the corresponding dry mass.

Approximately 12 hours before hydrothermal treatment, the samples were pre-soaked in the desired medium by subjecting them to vacuum cycles until saturation. Different pre-soaking liquids were chosen to assess the effects of acid concentration (distilled water, H_2SO_4 0.3 % m/m, and H_2SO_4 0.6 % m/m). As an alternative to standard acidic conditions, an alkaline medium (NaOH 0.6 % m/m) was also tested. The conditions of each test are summarized in Table 1. The saturated dimensions of the samples before the test were measured using a laser sensor (Bullier Automation M5L/4). There were three main reasons for using saturated samples: assurance of good heat transfer throughout the samples and prevention of changes in the viscoelastic properties and, more importantly, any mechanosorptive effects of wood due to changes in moisture content during the test.

2.2. Rheological measurements

The viscoelastic properties were measured using an in-house developed device, whose features and working principles have been presented in previous papers (Lancha et al., 2020; Mokdad et al., 2018). It has a dual-chamber reactor which allows mechanical tests to be accurately performed under high temperature and water-saturated conditions. The upper chamber is kept at room temperature to house the instrumentation system: i) a Newport LTA-HL actuator (travel range of 25 mm, a minimum incremental motion of 0.05 µm and accuracy of 3 µm) equipped with a displacement sensor; and ii) a load cell (MEASUREMENT SPECIALTIES XFTC 310). The sample is treated in the bottom chamber, which is, therefore, subjected to high temperatures and saturated steam conditions. The chambers are connected by a patented system (Placet and Perré, 2006), enabling a mechanical link between the two chambers without friction, a prerequisite for reliable force measurements. The transmission of the load from the actuator (located in the cold chamber) to the sample (located in the hot chamber) is ensured by a vertical moving rod. A plate, lying at the end of this rod, subjects the sample to compressive stress. Prior to each test, 100 mL of liquid water were added to the bottom of the chamber. During the heating-up phase, water vaporization ensured a water saturated atmosphere and condensation at the surface of the sample ensured its full saturation during the test.

Different continuous mechanical tests on biomass under compression can be performed with this device. This study focuses on the evolution of two parameters during the hydrothermal treatment: i) apparent modulus of elasticity (MOE) and ii) stress relaxation measured under compression.

At the beginning of the experiment, the sample is placed on the sample holder, and the reaction chamber is closed. The software is then launched for the experimental assay. Each test is composed of the following phases:

1. Heating (8 °C/min) from room temperature to the desired temperature using two electric heating collars (total of 370 W) placed at the outer surface of the chamber. The temperature was measured by a K-thermocouple near the sample and controlled by a PID system (Eurotherm 3216).
2. Maintaining the treatment temperature for 150 minutes
3. Cooling to room temperature by two external fans at approximately 9 °C/min

The mechanical properties of the samples were measured throughout the test according to the following cyclic protocol, repeated every 75 seconds:

1. **Offset of the load cell** in the absence of contact, allowing the sensor drift to be corrected, which is important as the applied force decreases at high temperature;
2. Slow (0.005 mm/s) displacement of the rod towards the sample;
3. **Contact detection** when the measured force reaches 0.05 N;
4. **Preload of the sample,** using compression until the preload force is reached (the targeted force depends on the temperature, and was determined during preliminary tests);
5. **MOE stage**, consisting of compression up to 0.5 % of deformation of the sample based on its initial water-saturated length;
6. **Viscoelastic stage**, relaxation for 30 seconds under constant deformation; and
7. Backward translation to release the contact and wait until the next cycle.

The stress levels applied in this protocol are intended to load the samples within the linear elasticity and viscoelastic ranges. The raw data obtained included the temperature of the chamber and the force and position of the actuator. The latter includes the additional deformations of the sample and the testing bench. To extract the sample deformation only, a series of blank tests were performed to quantify the deformation of the bench (without sample) as a function of the applied force. For a given force, it is then possible to calculate the portion of the deformation strictly related to the sample.

After blank correction and knowing the original sample dimensions, the stress and strain values are calculated:

$$\sigma = \frac{F}{S} \quad (1)$$

in which σ is the stress level (in Pa), F is the force measured by the load cell (in N), and S is the initial cross-sectional area of the sample (in m²).

$$\varepsilon = \frac{\Delta L}{L_0} \quad (2)$$

In which the strain (ε) is the dimensionless ratio between the sample deformation (ΔL) and the initial sample length (L_0).

The MOE is then determined by linear regression between the values of calculated stress and blank-corrected strain during the linear phase:

$$MOE = \frac{\Delta\sigma}{\Delta\varepsilon} = \frac{\Delta F}{\Delta L}\frac{L_0}{S} \quad (3)$$

Concerning the stress relaxation phase, results are expressed in terms of normalized stress levels (Eq. 4) as a function of relaxation time, in which σ_0 is the stress level at the beginning

of relaxation. To express the temporal evolution of normalized stress, the following expression is proposed, from which two parameters can be obtained: the recoverable part of the asymptotic value (α) and the characteristic time of relaxation (τ) (Mokdad et al., 2018).

$$\frac{\sigma_{(t)}}{\sigma_0} = 1 - \alpha \left(1 - e^{\frac{-t}{\tau}}\right) \quad (4)$$

For each repetition, α and τ were fit to the data using the Nelder-Mead method. Equation 4 was then used to calculate the dimensionless stress at the end of the relaxation interval (t = 30 s), R_{30}.

$$R_{30} = \frac{\Delta\sigma}{\sigma_0} = \frac{\sigma_0 - \sigma_{(t=30\ s)\ calculated}}{\sigma_0} = 1 - \frac{\sigma_{(30)}}{\sigma_0} \quad (5)$$

This data analysis allows the signal noise to be averaged at best over the 30-second interval.

2.3. Treatment conditions

Treatments were performed at 150, 160, and 180 °C, and the mechanical properties of wood were measured in the radial (R) and tangential (T) directions. All treatment conditions are summarized in Table 1. Sodium hydroxide and sulfuric acid concentrations were chosen based on previous studies (Kim et al., 2016; Youssef et al., 2017).

2.4. Chemical analysis

After treatment, the liquid fraction was recovered, and its volume was measured. It was then analyzed for sugars, organic acids and sugar degradation products. Quantification of sugars and organic acids was carried out on an Ultima 3000 HPLC (THERMO FISHER SCIENTIFIC) coupled with a Refractive Index Detector RI-101 (SHODEX). Separation was achieved on an Aminex HPX-87H column (300 x 7.8 mm) from Biorad at 30 °C. A mobile

phase of 2 mM of sulfuric acid (VWR) at a flow rate of 0.5 mL/min was used in isocratic mode and the injection volume was 10 µL. Total run analysis was 30 minutes. Components were identified by comparison of their retention time with standard solutions. Quantification was achieved using the area of the peak in external calibration, the range of concentration was from 0.2 to 10 g/L. Quantification of furfural and 5-(hydroxymethyl)furfural (HMF) were carried out on an Ultima 3000 HPLC (THERMO FISHER SCIENTIFIC) coupled with an UV Detector. Separation was achieved on an Acclaim Polar Advantage II C18 column (4.6 x 150 mm, 3 µm, 120 Å) from THERMO FISHER SCIENTIFIC. Column temperature was maintained at 30 °C. The mobile phase was a mixture of two solvents. Solvent A: Milli-Q water; and solvent B: Acetonitrile (SIGMA-ALDRICH) at a flow rate of 0.3 mL/min. Elution was achieved in gradient mode with an initial composition of 80 % of A and 20 % of B, held for 5 minutes. Proportion of B was then gradually increased to 99 % in 10 minutes and held at 99 % for 5 minutes, followed by going back to initial composition and stabilization of the column for 10 more minutes, summing a total run analysis of 30 minutes. Injection volume was 5 µL. Degradation products were identified by comparison of their retention time and of their UV spectra with standard solutions of HMF (SIGMA-ALDRICH) and furfural (SIGMA-ALDRICH). UV spectra were recorded from 200 to 380 nm, quantification of HMF and furfural was done at 277.8 and 285.5 nm respectively, which corresponds to their maximum of absorption. Quantification was achieved using the area of the peaks in external calibration, the range of concentrations was from 0.1 to 30 mg/L. Oligosaccharides concentrations were determined from the difference of monomeric sugars concentrations measured before and after an analytical hydrolysis step (Sluiter et al., 2008). To do so, 72 % H_2SO_4 to obtain an acid concentration of 4 %. The solution was then autoclaved at 121 °C for 1 hour.

Solid residue was washed with distilled water and had its dry mass determined. The mass loss during treatment was then calculated according to the following expression:

$$ML\ (\%) = \frac{M_0 - M}{M_0}.100 \qquad (6)$$

2.5. Fourier transform infrared (FTIR) analysis

FTIR analysis of native and hydrothermally treated samples was performed using a Spectrum Two FTIR Spectrometer (PerkinElmer) combined with an ATR unit . Spectra were recorded in the range from 4000 to 400 cm^{-1}, with an accumulation of 16 scans. All spectra had their baseline corrected prior to spectral analysis.

3. Results and Discussion

3.1. MOE

3.1.1. Effect of temperature and wood direction

Figure 1 reports typical apparent MOE results obtained with distilled water in the radial (left column) and tangential (right column) directions for the three plateau temperatures (150, 160, and 180 °C). At the beginning of each test, the MOE was measured at room temperature. The mean MOE value was 843 ± 13 MPa in the radial direction and 335 ± 97 MPa in the tangential direction. All results are presented as the dimensionless ratio between the MOE measured at a given time and the mean MOE value at room temperature. The evolution of the dimensionless MOE is plotted as a function of time (Figure 1a-d) and as a function of temperature (Figure 1 e-f).

During the heating phase, a strong MOE decrease was observed until the treatment temperature was reached (Figure 1a-b). Consistently during this phase, the tests conducted

at different temperatures superpose, as the heating rate is the same for all tests. The same trend is observed for either radial or tangential directions: regardless of the direction, approximately 97 % of the MOE initial value is lost at 150 °C. These observations take place during ca. the first 20 minutes of treatment (heating-up phase), highlighted by vertical solid lines in Figure 1a-b. This phase is, therefore, better observed when the apparent MOE is plotted against temperature (Figure 1e-f). In these plots, a difference between directions is observed in the shape of the curves. The MOE of samples loaded in the tangential direction decreased somewhat linearly with temperature, whereas radial tests demonstrated linear behavior only over a limited range of temperatures.

Once the plateau is reached—after 9, 21, and 23 minutes of treatment for a plateau temperature of 150, 160, and 180 °C, respectively—a second phase starts, during which changes occur at a constant temperature. In the radial direction (Figure 1c), whatever the duration of the plateau, a higher treatment temperature resulted in a lower MOE. At the beginning of the plateau, for example, the measured MOE represented only 0.028, 0.022, and 0.011 of its initial value for treatments at 150, 160, and 180 °C, respectively. At a given temperature, however, the evolution of the dimensionless MOE was not always monotonic. At 150 °C, the MOE decreased to a minimum of 0.018 after 97 minutes of treatment (88 minutes from the beginning of the plateau) and then slowly increased up to a maximum of 0.020 at the end of the treatment. The same behavior occurred faster for the treatment at 160 °C. The minimum value (0.016) was reached at approximately 50 minutes (29 minutes from the beginning of the plateau), after which values increased up to 0.018 at the end of the treatment. Finally, the treatment at 180 °C demonstrated even more complex behavior: the apparent MOE decreased quite rapidly down to 0.009 at minute 29, only 6 minutes after the beginning of the plateau. Then, it regained the same value as at the beginning of the

plateau (0.011) at minute 50 (17 minutes from the beginning of the plateau). The remaining portion of the test depicts a slow and regular decrease until the end (minimum of 0.008). In the tangential direction (Figure 1d), dimensionless MOE values at the beginning of the plateau were 0.023, 0.022, and 0.012 at 150, 160, and 180 °C, respectively. Minimum values were reached earlier than in the radial direction. At 150 °C, the minimum dimensionless MOE (0.016) was reached after 48 minutes (39 minutes from the beginning of the plateau), whereas, at 160 °C, it required 45 minutes (24 minutes from the beginning of the plateau) to reach the same minimum. For the treatment at 180 °C, after the beginning of the temperature plateau, the MOE value increased to a stable value of approximately 0.012 between 50 and 100 minutes (between 27 and 77 minutes from the beginning of the plateau, respectively) and then decreased to a minimum of ca. 0.010 at the end of the treatment.

3.1.2. Effect of pre-soaking media

Figure 2 shows typical MOE results obtained from poplar samples in the radial direction during hydrothermal treatment at 160 °C (a, c, e) and 180 °C (b, d, f), in which the effects of four different pre-soaking liquids were compared: distilled water, NaOH (0.6 % m/m), and H_2SO_4 (0.3 and 0.6 % m/m). As in section 3.1.1, results are represented as dimensionless MOE, using the mean radial MOE values measured at room temperature in water-saturated conditions as the reference value. As in Figure 1, Figure 2 depicts the evolution of dimensionless MOE versus time (a-d) and temperature (e-f).

Samples saturated with sodium hydroxide and sulfuric acid solutions presented lower MOE at room temperature than those saturated with distilled water (Figure 2e,f).

Sodium hydroxide yielded the lowest dimensionless MOE (approximately 0.1) at room temperature. These values further decreased to 0.015 and 0.011, respectively, at 160 and 180 °C when the plateau was attained. The behavior observed for NaOH-treated samples was then very different for treatments at 160 °C and 180 °C. Although at 180 °C MOE values seem to stagnate at 0.011, the behavior at 160 °C is similar to that of water-treated samples. MOE decreased to 0.012 and then increased again to almost the same value observed at the beginning of the plateau (0.015). The MOE of samples treated with NaOH remained the lowest until ca. 150 °C when they were reached in the 0.6 % H_2SO_4 treatments. Compared to samples treated with water, NaOH resulted in lower MOE values during the entire plateau for the 160 °C treatment. In contrast, at 180 °C, the MOE values were higher than those of the water treatment.

At 160 °C, the presence of H_2SO_4 caused a continuous reduction of MOE during the temperature plateau (Figure 2c-f), which was even more pronounced at higher H_2SO_4 concentration. At 180 °C, however, increasing the acid concentration caused almost no difference in the MOE. Indeed, both acid concentrations caused a loss of MOE with the same asymptotic value at 0.5 % for the dimensionless MOE, which represents a 200-fold division of the MOE at room temperature. Regardless of the temperature and the concentration, sulfuric acid resulted in lower MOE than water at the end of the treatment.

Finally, as expected, in all tested conditions, the use of a higher treatment temperature resulted in lower MOE. For samples treated with NaOH, however, only a slight difference was observed between the temperatures (160 and 180 °C).

3.2.Stress relaxation

After each linear loading, the stress relaxation of samples was monitored for 30 seconds. Figure 3 shows typical stress relaxation results of poplar samples during two different phases of the treatment: the heating-up phase (Figure 3a), for which results are expressed in terms of temperature, and the temperature plateau (Figure 3b), for which results are expressed in terms of treatment duration from the beginning of the plateau. The results shown in Figure 3 were obtained from a water-saturated sample treated at 160 °C and loaded in a radial direction. Experimental points are plotted as markers, and the best fit using Equation 4 is represented by dashed lines.

During the heating-up phase (Figure 3a), as the temperature increased from 17 °C to 54 °C, a significant increase in relaxation was observed. This trend is then inverted as the temperature continues to rise (curves at 77 °C and beyond). During this second period, the curves shifted upwards, revealing a reduction in viscoelasticity (results in green and yellow in Figure 3a). This trend continued once the temperature reached the plateau (curves evolving from yellow to pink in Figure 3b).

The parameters of Equation 4 were then used to calculate the normalized stress relaxation after 30 seconds (R_{30}), as described by Equation 5, to be explored in the following sections.

3.2.1. Effect of temperature and wood direction

Figure 4 displays the evolution of R_{30} as a function of time (Figure 4a,b) and temperature (Figure 4c,d) for different temperatures (150, 160, and 180 °C) in radial (left column) and tangential (right column) directions. The dashed lines represent the temperature, and the vertical lines indicate the beginning of the temperature plateau. For improved visualization of the results, results in Figure 4a,b were filtered using a 3-point sliding median.

During the heating-up phase (Figure 4c,d), the evolution of R_{30} confirms the trend observed on the raw relaxation curves. When heated from room temperature to approximately 60 °C, R_{30} increases up to a maximum of 0.020 in the radial direction and 0.018 in the tangential direction. From this point, a continuous decrease is observed. The superposition of the results of different tests validates the repeatability, despite the extreme difficulty of such measurements. Once the temperature plateau was reached, R_{30} values were almost twice as high in a radial direction than those in a tangential direction. During this period, in a radial direction, the effect of temperature was noticeable, as the highest value was obtained at 180 °C, followed by 160 °C, and finally, 150 °C. At 150 °C, the relaxation was approximately 0.024, and almost no change was observed throughout the temperature plateau (Figure 4c). At 160 °C, the plateau started at 0.038 and was the same as the results of the 150 °C test (R_{30} = 0.024) after 75 minutes of treatment (54 minutes from the beginning of the plateau). During the 180 °C test, the R_{30} plateau started at 0.056 and regularly decreased to reach 0.015 at the end of the treatment. Similar trends were obtained in the tangential direction (Figure 4d), except for substantially smaller values of R_{30}.

3.2.2. Effect of pre-soaking liquid

The effect of different pre-soaking liquids on the viscoelastic properties of poplar during hydrothermal treatment was also assessed. Using the same protocol as in the previous section, tests were performed in a radial direction at 160 °C (Figure 5a,c) and 180 °C (Figure 5b,d). The identified R_{30} values are shown in Figure 5 as a function of time (a-b) and temperature (c-d). In Figure 5a-b, the beginning of the temperature plateau is highlighted by the vertical black line, while the temperature is plotted as dashed lines. As in Figure 4a-b, Figure 5a-b presents filtered results (3-point sliding median).

During the heating-up phase (observed in Figure 5c,d), different pre-soaking media appeared to have a similar effect on the R_{30} parameter, as previously observed for water-only treatment, i.e., an initial increase of R_{30} up to a maximum value at around 60 °C and followed by a decrease. Notably, during this phase, the test with acid allowed the highest R_{30} values to be obtained until the plateau temperature. Sodium hydroxide and water, in contrast, resulted in lower R_{30} values during the same period.

For H_2SO_4-soaked samples, regardless of the concentration and the temperature, R_{30} seemed to behave monotonously during the temperature plateau (Figure 5c-d), regularly decreasing with time. In both 160 and 180 °C treatments, water produced the highest R_{30} values throughout this phase. A slight reduction of R_{30} can be observed at the highest temperature (180 °C vs. 160 °C), regardless of the reaction liquid. An exception to this trend was found when using NaOH: samples treated with this soaking liquid caused almost no reduction in MOE during the temperature plateau, and little behavior difference can be observed between samples treated at 160 °C and 180 °C.

3.3. Analysis of the FTIR-ATR spectra

Biomass chemical properties prior and after treatment were assessed through FTIR spectroscopy. For interpreting the results and assessing biomass different characteristics of biomass, three peak ratios previously described on the literature (Auxenfans et al., 2017) were used. Firstly, the lateral order index (LOI), used as an empirical crystalline index. It is defined as a ratio between the bands at 897 and 1423 cm^{-1} representing, respectively, the glycosidic bond in cellulose and the amount of crystalline cellulose. Secondly, the hydrogen bond intensity (HBI). Calculated from the ratio between the peaks at 3400 cm^{-1} (O-H stretching, hydrogen bonds) and 1323 cm^{-1} (CH rocking vibration of the glucose ring), it is

likely to represent the crystallinity as well as the amount of bound water of the biomass. Finally, the cross-linked lignin ratio (CLL) uses the bands at 1600 (stretching of the C=C and C=O aromatic lignin) and 1508 cm^{-1} (deformation of lignin CH2 and CH3) as an indicator of the proportion between condensed and cross-linked lignins. The obtained ratios are shown in Table 2, as well as the proportional change as related to native biomass (*values in italic*).

3.4. Qualitative results

Consistent with published studies, the sample color shifts from light to dark brown with increasing treatment severity, a cumulative effect of temperature level and acid concentration (Ewanick and Bura, 2010; Negro et al., 2003; Sun et al., 2005). Furthermore, samples pre-soaked with sodium hydroxide maintained a light brown color, which may be seen as the opposite effect caused by acidity. Qualitative and morphological features can provide valuable information on biomass chemical modifications, as shown in previous studies (Zoghlami et al., 2019).

3.5. Dynamics of chemical modifications

During hydrothermal treatment, two phenomena contribute to the changes observed on the mechanical properties of biomass: thermal activation and chemical degradation (Mokdad et al., 2018). Thermal activation of the viscoelastic behavior occurs during the heating-up phase, when the temperature increase leads to greater mobility of macromolecules. The switch from a glassy state to a rubbery state is known for its great impact on the mechanical properties of polymers (Olsson and Salmén, 1992). The transition is not as immediate for wood due to its complex mixture of multiple macromolecules. In the case of water-saturated wood, it is generally accepted that the temperature of glass transition ranges between 60 and 90 °C, which is mainly attributed to the glass transition of lignins (Irvine, 1985; Olsson

and Salmén, 1992; Salmén, 1984). This results in a substantial loss of rigidity, characterized by a decrease in the apparent MOE and higher relaxation (Assor et al., 2009; Fahlén and Salmén, 2003; Mokdad et al., 2018; Placet et al., 2008, 2007).

Previous works have linked some of the chemical modifications that occur during hydrothermal treatment to the mechanical properties of biomass (Assor et al., 2009; Mokdad et al., 2018; Navi and Stanzl-Tschegg, 2009). Lignin and, more precisely its glass transition, is usually singled out as the major factor responsible for the viscoelastic behavior of wood, especially with regard to thermal activation (Irvine, 1985). Nevertheless, some studies have found evidence of the importance of hemicellulose on the mechanical behavior of wood (Bergander and Salmén, 2002; Zhang et al., 2016). Consistent with the present results, hemicellulose-free samples presented less viscoelasticity than native wood (Navi and Stanzl-Tschegg, 2009; Zhang et al., 2016). Furthermore, Mokdad et al. (2018) observed a reduction of stress relaxation during hydrothermal treatment and attributed it to the re-condensation of lignins. Hence, both hydrolysis and repolymerization should result in a decrease in stress relaxation with increased residence time.

An inverse relationship has been observed for rigidity. While hydrolysis reactions tend to reduce wood rigidity, the formation of condensed lignin linkages increases rigidity (Assor et al., 2009). This observation is related to the degree of polymerization of molecules. Cleaved chains have a reduced mechanical role, which lowers the apparent rigidity (Dwianto et al., 1999).

The combination of our mechanical measurements (apparent MOE and relaxation) is consistent with the mechanisms described above. The water-soaked samples analyzed in a tangential direction, for example, showed a linear decrease of MOE with temperature during

the heating-up phase (Figure 1b). In the radial direction (Figure 1a), a regular decrease was also observed, even though the trend is not linear. This is probably due to the presence of different morphological structures (fibers and rays) acting in radial direction and which are not activated in the same way. Regardless of the direction (Figure 1a-b), the results from all three treatments (150, 160, and 180 °C) merged into a single master curve. Similar observations made in previous studies were attributed to the thermal activation of the viscoelastic behavior of wood (Mokdad et al., 2018). While thermal activation is undoubtedly one of the mechanisms involved in the reduction of rigidity during this phase, the evolution of relaxation (Figure 3a-b) implies that another phenomenon is occurring simultaneously. The first part of the heating-up period, with a concomitant decrease of MOE and an increase of relaxation, can be readily explained by thermal activation. This is not consistent once the maximum value of relaxation, at ca. 60 °C, has been reached. After this point, the apparent modulus continues to decrease while relaxation decreases instead of increasing. These facts indicate that, even at such low temperatures, there could be some chemical degradation, a phenomenon that would have been hidden if only stiffness had been measured. Evidence of chemical degradation at 80–90 °C has been previously revealed, and the importance of water as an activating agent of degradation reactions has been highlighted (Placet et al., 2008). Considering the temperature level, the hydrolysis of hemicelluloses is the most probable mechanism (Lancha et al., 2020; Placet et al., 2008).

During treatment at constant temperature (Figure 1a,b, and Figure 3a,b), the evolution of the mechanical behavior is solely related to chemical degradation, as mechanical and treatment times have been distinguished through cyclic loading. The monotonous decrease of relaxation (Figure 3c-d) can be attributed to both hydrolysis and condensation reactions, as their effects are additive (Mokdad et al., 2018). On the contrary, hydrolysis reactions are

likely to reduce MOE during the first minutes of the plateau, while condensation would be responsible for its subsequent increase (Assor et al., 2009). The opposite effects of these two phenomena are likely to explain the trends observed in Figure 1c-d. These trends are confirmed by the FTIR results (Table 2), that depict a clear increase of the CLL for treatments at 150 °C and 160 °C (0.61 and 0.58, respectively), possibly indicating the prevalence of re-condensation reactions at the final stages of treatment plateau. For severe treatment (180 °C), however, a somewhat continuous decrease in the MOE was observed with residence time. Two phenomena could explain this result. Firstly, a degradation of the newly formed condensed lignin structures. The CLL ratio (Table 2) seems to support this hypothesis, since treatment at 180 °C presents a lower CLL (0.49) then those at 150 and 160 °C. Secondly, a higher treatment temperature is likely to introduce a new phenomenon into the balance: cellulose depolymerization (Garrote et al., 1999; Jacquet et al., 2011; Mokdad et al., 2018; Vila et al., 2013). This hypothesis is supported by the results of mass loss (Table 1). Whilst treatments at 150 and 160 °C exhibit close mass loss values (31.2 and 32.7%, respectively), the treatment at 180°C causes a mass loss of 41.5% for the same period of time. The FTIR results (Table 2) provide additional insight in this respect. A considerable reduction in the HBI ratio indicates a less organized structure and, thus, a possible loss of crystallinity. The results of Vila et al. (2013), revisited by Mokdad et al. (2018), showed a clear effect of treatment temperature on the reduction of the degree of polymerization (DP) of cellulose. While at 180 °C, the DP decreased by 75 % after 150 minutes of treatment (equivalent to the end of the plateau in our study), the loss was only by 25 % at 160 °C. The length of cellulose chains is, thus, a major factor influencing the MOE of samples treated at high temperature. To a lesser extent, increasing the severity of the treatment could favor depolymerization to the detriment of re-condensation. Indeed, the high water availability

and the severe conditions to which biomass was subjected during this study are prone to promote the hydrolytic pathway of lignin degradation, leading to the formation of Hibbert ketones and limiting re-condensation of lignin (Obame et al., 2019; Samuel et al., 2013).

Pre-soaking in specific liquids also affected the data trends. Soaking in sodium hydroxide at room temperature for 12 hours reduced the initial MOE by approximately a factor of ten (Figure 2a-b). Despite this considerable initial decrease, the module stagnates during the temperature plateau (Figure 2c-f). A similar observation can be made for relaxation. With sodium hydroxide, the relaxation reduced very rapidly as the temperature approached the plateau, as shown by an acceleration of the decrease of R_{30} (Figure 5c,d), but remained almost constant afterward, during the plateau (Figure 5a,b). The mechanisms involved in alkali pretreatments are different from those previously described for acid pretreatments. Sodium hydroxide has been proven to effectively promote the cleavage of ether and ester bonds of lignin-carbohydrate complexes (LCC) and of lignin C–C bonds (Kim et al., 2016), even at room temperature (Wu et al., 2011). The pretreatment protocol used in this study, which includes an overnight pre-soaking step, could, therefore, promote early lignin and hemicellulose solubilization (Kim et al., 2016). The reduction observed in CLL values (Table 2) for samples pre-soaked in sodium hydroxide supports the hypothesis of lignin solubilization. Furthermore, an alkali medium promotes saponification of acetyl and uronic ester groups of hemicelluloses, which limits autohydrolysis processes usually observed under acidic conditions or water (Chen et al., 2013). The presence of C5 oligosaccharides in the treatment liquid corroborates the evolution of mechanical properties (Figure 6). Similar observations have been made by Chadni et al. (2019) when evaluating the effect of the pH of the pre-soaking liquid on the steam explosion of spruce sawdust. The use of sodium hydroxide resulted in hemicelluloses with significantly higher molecular weights than those treated

only with water. These facts are consistent with our macroscopic results, in which almost no changes on the mechanical properties were observed during the temperature plateau for samples treated with sodium hydroxide. This could help understand why only a slight difference is observed between samples pre-soaked with sodium hydroxide and treated at 160 and 180 °C. Indeed, the greatest effect of this pre-soaking liquid seems to be lignin extraction prior to the treatment rather than during the plateau temperature. The light brown color of the samples after the treatment also supports this mechanism. Hydrothermally treated samples are usually expected to be darker, due to several mechanisms, such as the breakdown of lignin and wood extractives, tannin and flavonoid condensation induced by lignin condensation, and reactions with furfural and 5-hydroxymethylfurfural (Ewanick and Bura, 2010; Negro et al., 2003; Sun et al., 2005). The lignin and hemicellulose extraction promoted by sodium hydroxide during sample saturation resulted in fewer degradation products and, consequently, a lighter color.

According to our measurements, the use of dilute acid as pre-soaking medium results in a monotonous decrease of both MOE and R_{30}. Following the above reasoning and given the fact that no module re-increase was observed during the plateau, it can be assumed that sulfuric acid favored cleavage rather than condensation of lignins. Furthermore, two different mechanisms have been observed for the cleavage of β-O-4' aryl ether linkages: the homolytic and the heterolytic pathways. In acidic conditions, the acid-catalyzed hydrolytic route prevails, leading to the formation of Hibbert ketones (Obame et al., 2019). For the same pretreatment conditions, dilute acid was found to enhance the depolymerization and solubilization of lignin into the liquid phase when compared to water-only pretreatments (Zhang et al., 2015).

The use of sulfuric acid as pre-soaking liquid also resulted in profound modifications of biomass carbohydrate fraction. In addition to furfural and HMF – already detected in the case of water-only treatments – high amounts of levulinic and formic acids were also observed. The presence of these molecules reflects extensive sugar degradation in both C5 and C6 fractions (Steinbach et al., 2017). The degradation and, thus, loss of the structural function of carbohydrates is in complete agreement with the mechanical results obtained at the macroscopic scale.

4. Conclusion

This study proposes a set of continuous rheologic measurements carried out during the hydrothermal treatment of poplar. Various treatment conditions were tested, including the temperature (150, 160, and 180 °C) and the soaking liquid (distilled water, acid solution, or alkaline solution). Thanks to chemical analysis performed on the treated solid and on the recovered liquid fraction, the concomitant evolution of stiffness and relaxation were analyzed in terms of thermal activation of viscoelasticity, cleavage of molecular linkages, and re-condensation. The two complementary mechanical properties measured in our protocol allowed us to draw meaningful conclusions regarding the chemical mechanisms involved in hydrothermal treatment.

5. Acknowledgments

This study was conducted in the Centre Européen de Biotechnologie et de Bioéconomie (CEBB), supported by Région Grand Est, Département de la Marne, Grand Reims, and the European Union. In particular, the authors would like to thank Département de la Marne for its financial support and the French Council for Poplar as well as Huberlant sawmill (Cormicy, France) for providing the wood used in this study.

6. References

1. Asada, C., Sasaki, C., Hirano, T., Nakamura, Y., 2015. Chemical characteristics and enzymatic saccharification of lignocellulosic biomass treated using high-temperature saturated steam: Comparison of softwood and hardwood. Bioresour. Technol. 182, 245–250. https://doi.org/10.1016/j.biortech.2015.02.005
2. Assor, C., Placet, V., Chabbert, B., Habrant, A., Lapierre, C., Pollet, B., Perré, P., 2009. Concomitant changes in viscoelastic properties and amorphous polymers during the hydrothermal treatment of hardwood and softwood. J. Agric. Food Chem. 57, 6830–6837. https://doi.org/10.1021/jf901373s
3. Auxenfans, T., Crônier, D., Chabbert, B., Paës, G., 2017. Understanding the structural and chemical changes of plant biomass following steam explosion pretreatment. Biotechnol. Biofuels 10, 36. https://doi.org/10.1186/s13068-017-0718-z
4. Barros, J., Serk, H., Granlund, I., Pesquet, E., 2015. The cell biology of lignification in higher plants. Ann. Bot. 115, 1053–1074. https://doi.org/10.1093/aob/mcv046
5. Bergander, A., Salmén, L., 2002. Cell wall properties and their effects on the mechanical properties of fibers. J. Mater. Sci. 37, 151–156. https://doi.org/10.1023/A:1013115925679
6. Chadni, M., Grimi, N., Bals, O., Ziegler-devin, I., Brosse, N., 2019. Steam explosion process for the selective extraction of hemicelluloses polymers from spruce sawdust. Ind. Crop. Prod. 141, 111757. https://doi.org/10.1016/j.indcrop.2019.111757
7. Chen, Y., Stevens, M.A., Zhu, Y., Holmes, J., Xu, H., 2013. Understanding of alkaline pretreatment parameters for corn stover enzymatic saccharification. Biotechnol. Biofuels 6, 1. https://doi.org/10.1186/1754-6834-6-8

8. Dwianto, W., Morooka, T., Norimoto, M., Kitajima, T., 1999. Stress relaxation of sugi (cryptomeria japonica d.don) wood in radial compression under high temperature steam. Holzforschung 53, 541–546. https://doi.org/10.1515/HF.1999.089
9. Ewanick, S., Bura, R., 2010. Hydrothermal pretreatment of lignocellulosic biomass, in: Waldron, K. (Ed.), Bioalcohol Production: Biochemical Conversion of Lignocellulosic Biomass. Woodhead Publishing, New Delhi, pp. 3–23. https://doi.org/10.1533/9781845699611.1.3
10. Fahlén, J., Salmén, L., 2003. Cross-sectional structure of the secondary wall of wood fibers as affected by processing. J. Mater. Sci. 38, 119–126. https://doi.org/10.1023/A:1021174118468
11. Garrote, G., Dominguez, H., Parajo, J.C., 1999. Hydrothermal processing of lignocellulosic materials. Holz als Roh- und Werkst. 57, 191–202. https://doi.org/10.1007/s001070050039
12. Haghighi Mood, S., Hossein Golfeshan, A., Tabatabaei, M., Salehi Jouzani, G., Najafi, G.H., Gholami, M., Ardjmand, M., 2013. Lignocellulosic biomass to bioethanol, a comprehensive review with a focus on pretreatment. Renew. Sustain. Energy Rev. 27, 77–93. https://doi.org/10.1016/j.rser.2013.06.033
13. Irvine, G.M., 1985. The significance of the glass transition of lignin in thermomechanical pulping. Wood Sci. Technol. 19, 139–149. https://doi.org/10.1007/BF00353074
14. Jacquet, N., Quiévy, N., Vanderghem, C., Janas, S., Blecker, C., Wathelet, B., Devaux, J., Paquot, M., 2011. Influence of steam explosion on the thermal stability of cellulose fibres. Polym. Degrad. Stab. 96, 1582–1588. https://doi.org/10.1016/j.polymdegradstab.2011.05.021

15. Jönsson, L.J., Martín, C., 2016. Pretreatment of lignocellulose: Formation of inhibitory by-products and strategies for minimizing their effects. Bioresour. Technol. 199, 103–112. https://doi.org/10.1016/j.biortech.2015.10.009
16. Kim, J.S., Lee, Y.Y., Kim, T.H., 2016. A review on alkaline pretreatment technology for bioconversion of lignocellulosic biomass. Bioresour. Technol. 199, 42–48. https://doi.org/10.1016/j.biortech.2015.08.085
17. Lancha, J.P., Colin, J., Guerin, C., Almeida, G., Perré, P., 2020. Shrinkage as a continuous indicator of chemical degradation of poplar wood during hydrothermal pretreatment. Manuscr. Submitt. Publ.
18. Lapierre, C., 1993. Application of New Methods for the Investigation of Lignin Structure, in: Jung, H.G., Buxton, D.R., Hatfield, R.D., Ralph, J. (Eds.), Forage Cell Wall Structure and Digestibility. American Society of Agronomy, Madison, pp. 133–166. https://doi.org/10.2134/1993.foragecellwall.c6
19. Lapierre, C., Pollet, B., Rolando, C., 1995. New insights into the molecular architecture of hardwood lignins by chemical degradative methods. Res. Chem. Intermed. 21, 397–412. https://doi.org/10.1007/BF03052266
20. Li, J., Henriksson, G., Gellerstedt, G., 2007. Lignin depolymerization / repolymerization and its critical role for delignification of aspen wood by steam explosion. Bioresour. Technol. 98, 3061–3068. https://doi.org/10.1016/j.biortech.2006.10.018
21. Limayem, A., Ricke, S.C., 2012. Lignocellulosic biomass for bioethanol production: current perspectives, potential issues and future prospects. Prog. Energy Combust. Sci. 38, 449–467. https://doi.org/10.1016/j.pecs.2012.03.002

22. Liu, S., Lu, H., Hu, R., Shupe, A., Lin, L., Liang, B., 2012. A sustainable woody biomass biorefinery. Biotechnol. Adv. 30, 785–810. https://doi.org/10.1016/j.biotechadv.2012.01.013
23. Mansfield, S.D., Kim, H., Lu, F., Ralph, J., 2012. Whole plant cell wall characterization using solution-state 2D NMR. Nat. Protoc. 7, 1579–1589. https://doi.org/10.1038/nprot.2012.064
24. Mokdad, S., Casalinho, J., Almeida, G., Perré, P., 2018. Assessment of biomass alterations during hydrothermal pretreatment by in- situ dynamic mechanical analysis. Biomass and Bioenergy 108, 330–337. https://doi.org/10.1016/j.biombioe.2017.11.014
25. Navi, P., Stanzl-Tschegg, S., 2009. Micromechanics of creep and relaxation of wood. A review. COST Action E35 2004-2008: Wood machining - Micromechanics and fracture. Holzforschung 63, 186–195. https://doi.org/10.1515/HF.2009.013
26. Negro, M.J., Manzanares, P., Oliva, J.M., Ballesteros, I., Ballesteros, M., 2003. Changes in various physical/chemical parameters of Pinus pinaster wood after steam explosion pretreatment. Biomass and Bioenergy 25, 301–308. https://doi.org/10.1016/S0961-9534(03)00017-5
27. Nitsos, C.K., Matis, K.A., Triantafyllidis, K.S., 2013. Optimization of hydrothermal pretreatment of lignocellulosic biomass in the bioethanol production process. ChemSusChem 6, 110–122. https://doi.org/10.1002/cssc.201200546
28. Obame, S.N., Ziegler-Devin, I., Safou-Tchima, R., Brosse, N., 2019. Homolytic and Heterolytic Cleavage of β-Ether Linkages in Hardwood Lignin by Steam Explosion. J. Agric. Food Chem. 67, 5989–5996. https://doi.org/10.1021/acs.jafc.9b01744

29. Olsson, A.-M., Salmén, L., 1992. Viscoelasticity of In Situ Lignin as Affected by Structure, in: Viscoelasticity of Biomaterials. pp. 133–143. https://doi.org/10.1021/bk-1992-0489.ch009
30. Passard, J., Perré, P., 2005. Viscoelastic behaviour of green wood across the grain. Part II. A temperature dependent constitutive model defined by inverse method. Ann. For. Sci. 62, 823–830. https://doi.org/10.1051/forest:2005088
31. Placet, V., Passard, J., Perré, P., 2008. Viscoelastic properties of wood across the grain measured under water-saturated conditions up to 135 °c: Evidence of thermal degradation. J. Mater. Sci. 43, 3210–3217. https://doi.org/10.1007/s10853-008-2546-9
32. Placet, V., Passard, J., Perré, P., 2007. Viscoelastic properties of green wood across the grain measured by harmonic tests in the range 0-95°C: Hardwood vs. softwood and normal wood vs. reaction wood. Holzforschung 61, 548–557. https://doi.org/10.1515/HF.2007.093
33. Placet, V., Perré, P., 2006. Chambre d'essai bi-climatique. Ref: BFF 06P0432. Ref: BFF 06P0432.
34. Salmén, L., 1984. Viscoelastic properties of in situ lignin under water-saturated conditions. J. Mater. Sci. 19, 3090–3096. https://doi.org/10.1007/BF01026988
35. Samuel, R., Cao, S., Das, B.K., Hu, F., Pu, Y., Ragauskas, A.J., 2013. Investigation of the fate of poplar lignin during autohydrolysis pretreatment to understand the biomass recalcitrance. RSC Adv. 3, 5305–5309. https://doi.org/10.1039/c3ra40578h
36. Shinde, S.D., Meng, X., Kumar, R., Ragauskas, A.J., 2018. Recent advances in understanding the pseudo-lignin formation in a lignocellulosic biorefinery. Green Chem. 20, 2192–2205. https://doi.org/10.1039/c8gc00353j

37. Sluiter, A., Hames, B., Ruiz, R., Scarlata, C., Sluiter, J., Templeton, D., 2008. Determination of sugars, byproducts, and degradation products in liquid fraction process samples, National Renewable Energy Laboratory. https://doi.org/NREL/TP-510-42623

38. Steinbach, D., Kruse, A., Sauer, J., 2017. Pretreatment technologies of lignocellulosic biomass in water in view of furfural and 5-hydroxymethylfurfural production- A review. Biomass Convers. Biorefinery 7, 247–274. https://doi.org/10.1007/s13399-017-0243-0

39. Sun, Q., Pu, Y., Meng, X., Wells, T., Ragauskas, A.J., 2015. Structural Transformation of Isolated Poplar and Switchgrass Lignins during Dilute Acid Treatment. ACS Sustain. Chem. Eng. 3, 2203–2210. https://doi.org/10.1021/acssuschemeng.5b00426

40. Sun, X.F., Xu, F., Sun, R.C., Fowler, P., Baird, M.S., 2005. Characteristics of degraded cellulose obtained from steam-exploded wheat straw. Carbohydr. Res. 340, 97–106. https://doi.org/10.1016/j.carres.2004.10.022

41. Trajano, H.L., Wyman, C.E., 2013. Fundamentals of biomass pretreatment at low pH, in: Aqueous Pretreatment of Plant Biomass for Biological and Chemical Conversion to Fuels and Chemicals. pp. 103–128. https://doi.org/10.1002/9780470975831.ch6

42. Vila, C., Francisco, J.L., Santos, V., Parajó, J.C., 2013. Effects of hydrothermal processing on the cellulosic fraction of Eucalyptus globulus wood. Holzforschung 67, 33–40. https://doi.org/10.1515/hf-2012-0046

43. Waldron, K., 2010. Bioalcohol production: Biochemical conversion of lignocellulosic biomass. Woodhead Publishing, New Delhi.

44. Wu, L., Arakane, M., Ike, M., Wada, M., Takai, T., Gau, M., Tokuyasu, K., 2011. Low temperature alkali pretreatment for improving enzymatic digestibility of sweet sorghum bagasse for ethanol production. Bioresour. Technol. 102, 4793–4799. https://doi.org/10.1016/j.biortech.2011.01.023

45. Wypych, G., 2016. The Effect of Fillers on the Mechanical Properties of Filled Materials, in: Wypych, G. (Ed.), Handbook of Fillers. ChemTec Publishing, Toronto, pp. 467–531. https://doi.org/10.1016/b978-1-895198-91-1.50010-5

46. Xiao, L.-P., Lin, Z., Peng, W.-X., Yuan, T.-Q., Xu, F., Li, N.-C., Tao, Q.-S., Xiang, H., Sun, R.-C., 2014. Unraveling the structural characteristics of lignin in hydrothermal pretreated fibers and manufactured binderless boards from Eucalyptus grandis. Sustain. Chem. Process. 2, 9. https://doi.org/10.1186/2043-7129-2-9

47. Youssef, Z., Ducept, F., Bennaceur, H., Malinowska, B., Almeida, G., Perre, P., Flick, D., 2017. Residence time distribution in a biomass pretreatment reactor: Experimentation and modeling. Chem. Eng. Res. Des. 125, 233–244. https://doi.org/10.1016/j.cherd.2017.07.015

48. Zhang, L., Yan, L., Wang, Z., Laskar, D.D., Swita, M.S., Cort, J.R., 2015. Characterization of lignin derived from water - only and dilute acid flowthrough pretreatment of poplar wood at elevated temperatures. Biotechnol. Biofuels 8, 1–14. https://doi.org/10.1186/s13068-015-0377-x

49. Zhang, S.Y., Fei, B.H., Wang, C.G., 2016. Effects of chemical extraction treatments on nano-scale mechanical properties of the wood cell wall. BioResources 11, 7365–7376. https://doi.org/10.15376/biores.11.3.7365-7376

50. Zoghlami, A., Refahi, Y., Terryn, C., Paës, G., 2019. Multimodal characterization of acid-pretreated poplar reveals spectral and structural parameters strongly correlate with saccharification. Bioresour. Technol. 293, 122015. https://doi.org/10.1016/j.biortech.2019.122015

8. Figure Captions

Figure 1. Modulus of elasticity of poplar as a function of time (a-d) and temperature (e-f) for different plateau temperatures. The left column (a, c, e) depicts radial tests and the right (b, d, f), tangential tests. Figures (c) and (d) are enlargements of the low values of MOE in figures (a) and (b). MOE measurements are represented by markers, while temperatures in the plot (a-d) are represented by dashed lines. Vertical solid lines highlight the beginning of the temperature plateau.

Figure 2. Modulus of elasticity as a function of time (a-d) and temperature (e,g) for two plateau temperatures: 160 °C (left column, a, c, e, g) and 180 °C (right column, b, d, f). In figures (c) and (d), the zoom scale of the y-axis is different as it was chosen to represent, at best, the notable trends.

Figure 3. Typical stress relaxation results of water-saturated poplar in a radial direction (a) as a function of different temperatures during the heating-up phase and (b) as a function of time during the plateau at 160 °C. For the sake of clarity, only one result out of two and six are represented in (a) and (b), respectively.

Figure 4. Relaxation ratio after 30 s of compression as a function of time (a, b) and temperature (c, d) for different plateau temperatures in the radial (left column) and tangential (right column) directions.

Figure 5. Dimensionless stress after 30 s of compression as a function of time (a, b) and temperature (c, d) for the tests at 160 °C (left column) and 180 °C (right column).

Figure 6. Chemical composition of the liquid fraction after treatment under different conditions. Liquid fraction was analyzed for oligosaccharides, monosaccharides, organic acids and sugar degradation products.

9. Tables and Figures

Table 1. Summary of the treatment conditions of all tests performed on poplar samples

Temperature (°C)	Direction	Reagent	Concentration (% m/m)	Initial pH	Final pH	Mass loss (%)
150	T	Water	-	-	3.17±0.01	31.2±3.6
160	T	Water	-	-	3.14±0.02	32.7±4.2
180	T	Water	-	-	3.15±0.01	41.5±5.3
150	R	Water	-	-	3.17±0.01	31.2±3.6
160	R	Water	-	-	3.14±0.02	32.7±4.2
180	R	Water	-	-	3.15±0.01	41.5±5.3
160	R	NaOH	0.6	12.57	10.30±0.01	53.4±7.8
160	R	H_2SO_4	0.3	1.51	1.62±0.03	62.8±3.3
160	R	H_2SO_4	0.6	1.29	1.54±0.03	75.3±9.4
180	R	NaOH	0.6	12.57	10.19±0.02	47.3±5.6
180	R	H_2SO_4	0.3	1.51	1.56±0.03	65.1±7.1
180	R	H_2SO_4	0.6	1.29	1.55±0.03	78.0±2.9

Table 2. FTIR Cellulose and lignin related properties of native and hydrothermally treated biomass and their relative change based on native values (italic).

	LOI (A_{1423}/A_{897})	HBI (A_{3400}/A_{1323})	CLL ($A_{1508}/_{1600}$)
Native	1.17	13.83	0.42
150° water	1.02 (-12.9 %)	13.61 (-1.6 %)	0.61 (43.9 %)
160°C water	1.06 (-9.2 %)	13.53 (-2.2 %)	0.58 (35.7 %)
180°C water	1.05 (-10.1 %)	10.45 (-24.4 %)	0.49 (15.1 %)
160°C NaOH	0.94 (-19.8 %)	8.60 ()-37.8 %	0.35 (-18.1 %)
160°C H_2SO_4 0.3%	1.51 (28.9 %)	13.22 (-4.4 %)	0.54 (28.2 %)
160°C H_2SO_4 0.6%	1.28 (9.7 %)	13.19 (-4.6 %)	0.61 (44.6 %)
180°C NaOH	0.90 (-22.6 %)	10.97 (-20.7 %)	0.34 (-21.3 %)
180°C H_2SO_4 0.3%	1.43 (22.1 %)	11.87 (-14.1 %)	0.43 (0.1 %)
180°C H_2SO_4 0.6%	0.99 (-15.2 %)	10.70 (-22.6 %)	0.66 (54.3 %)

Figure 1:

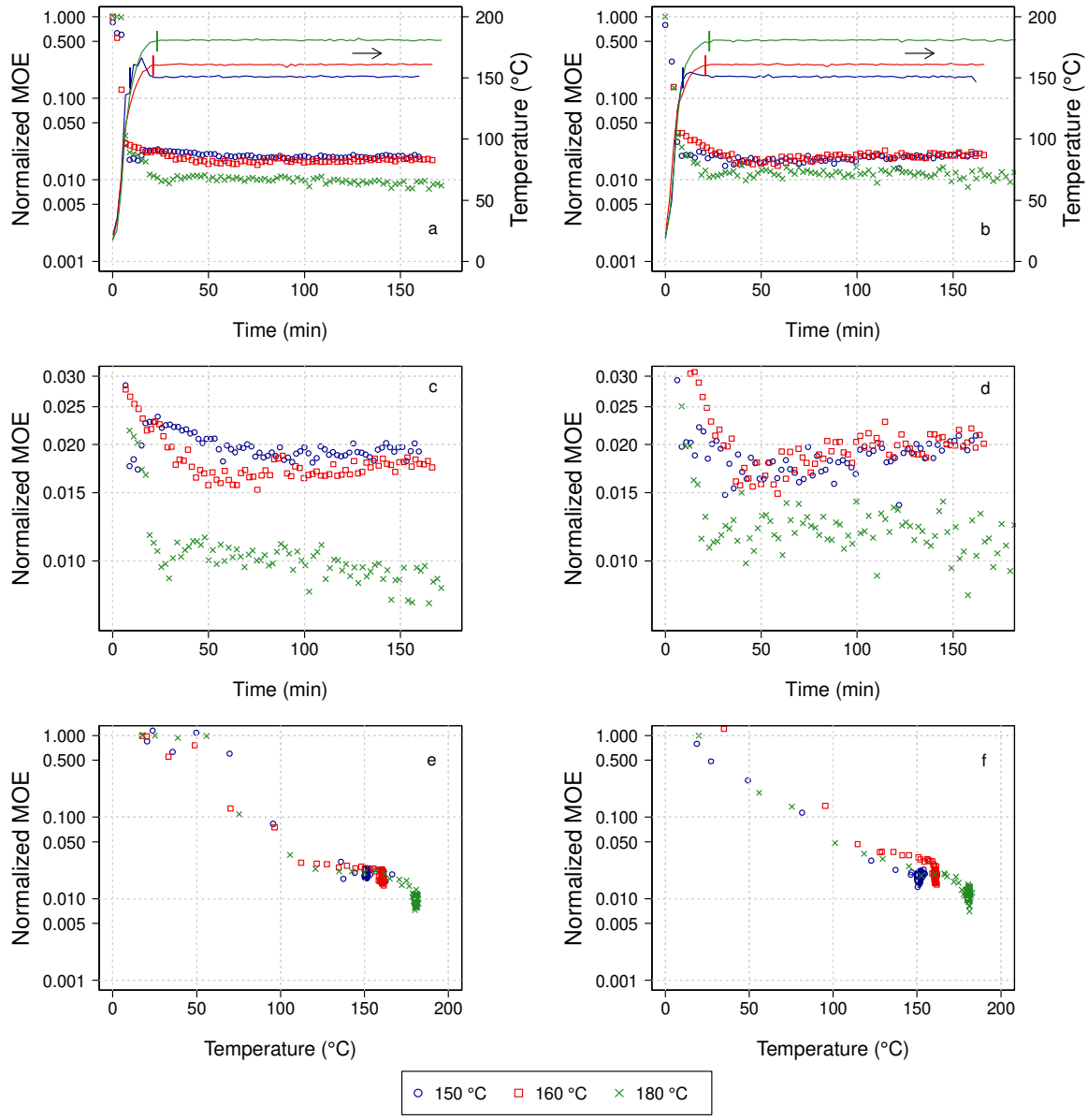
Normalized MOE
Temperature (°C)
Time (min)
Temperature (°C)
a
b
c
d
e
f
150 °C
160 °C
180 °C

Figure 2:

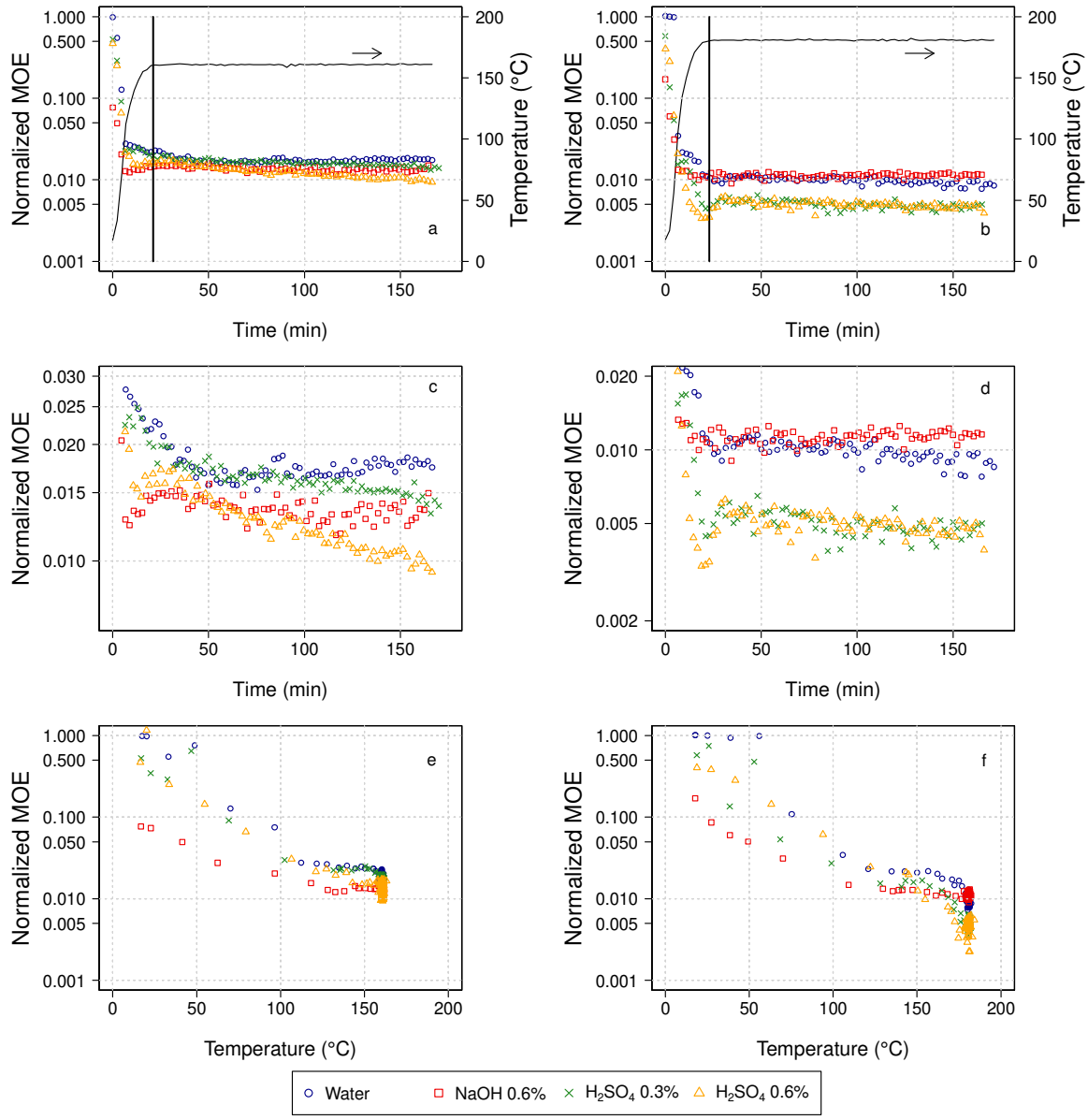
Normalized MOE
Temperature (°C)
Time (min)
a
b
c
d
e
f
Water
NaOH 0.6%
H2SO4 0.3%
H2SO4 0.6%

Figure 3:

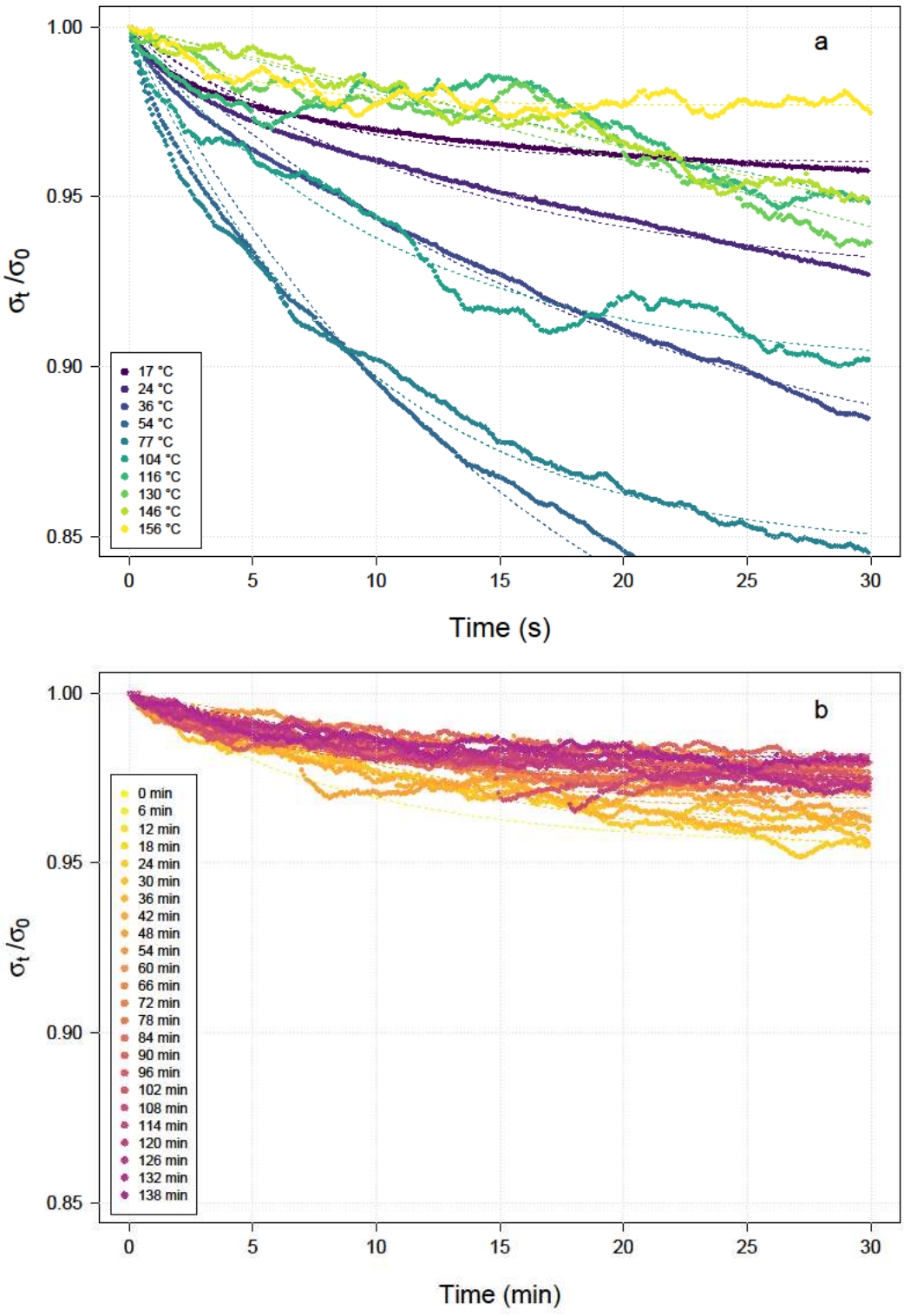
a
1.00
0.95
0.90
0.85
σ_t / σ_0
17 °C
24 °C
36 °C
54 °C
77 °C
104 °C
116 °C
130 °C
146 °C
156 °C
0
5
10
15
20
25
30
Time (s)
b
1.00
0.95
0.90
0.85
σ_t / σ_0
0 min
6 min
12 min
18 min
24 min
30 min
36 min
42 min
48 min
54 min
60 min
66 min
72 min
78 min
84 min
90 min
96 min
102 min
108 min
114 min
120 min
126 min
132 min
138 min
0
5
10
15
20
25
30
Time (min)

Figure 4:

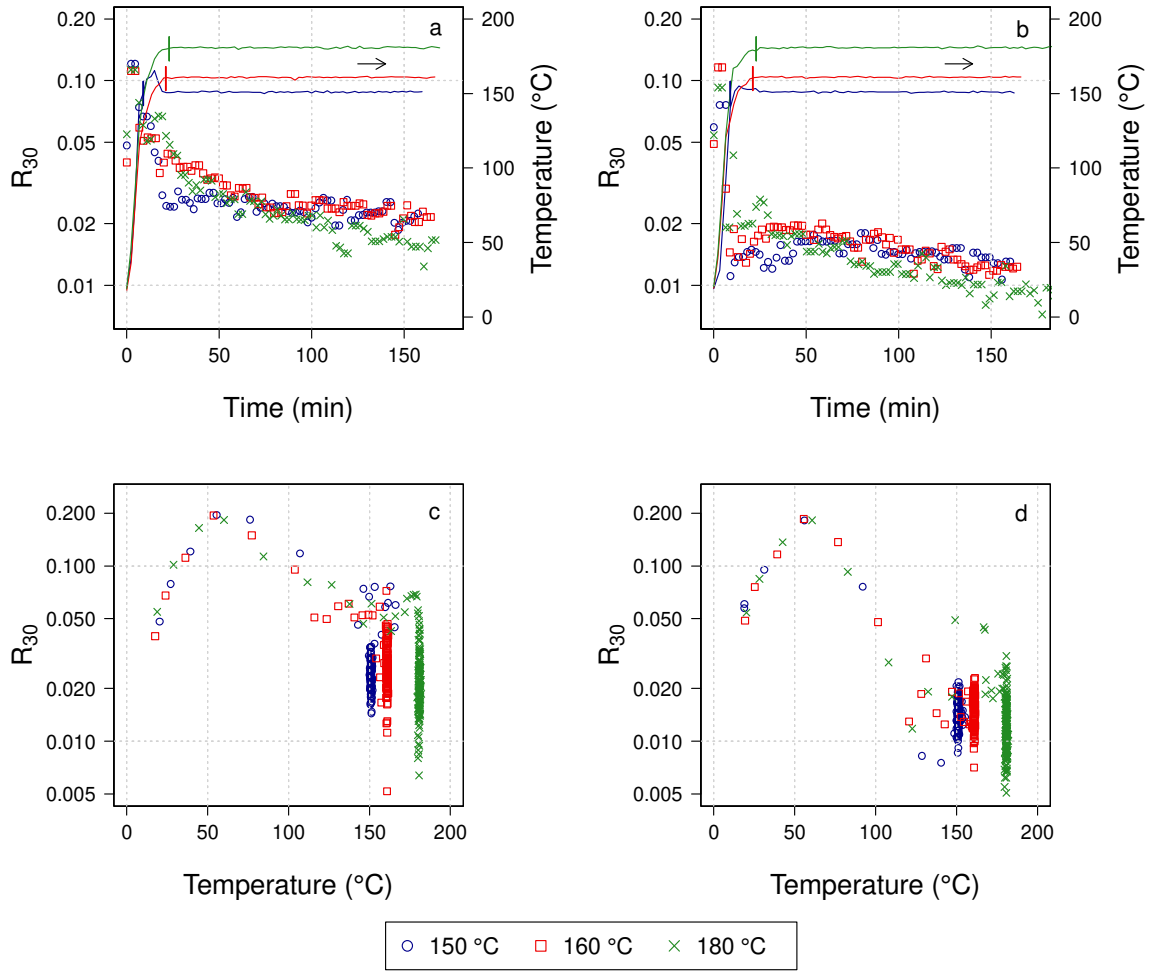
a
b
c
d
R30
Temperature (°C)
Time (min)
Temperature (°C)
150 °C
160 °C
180 °C

Figure 5:

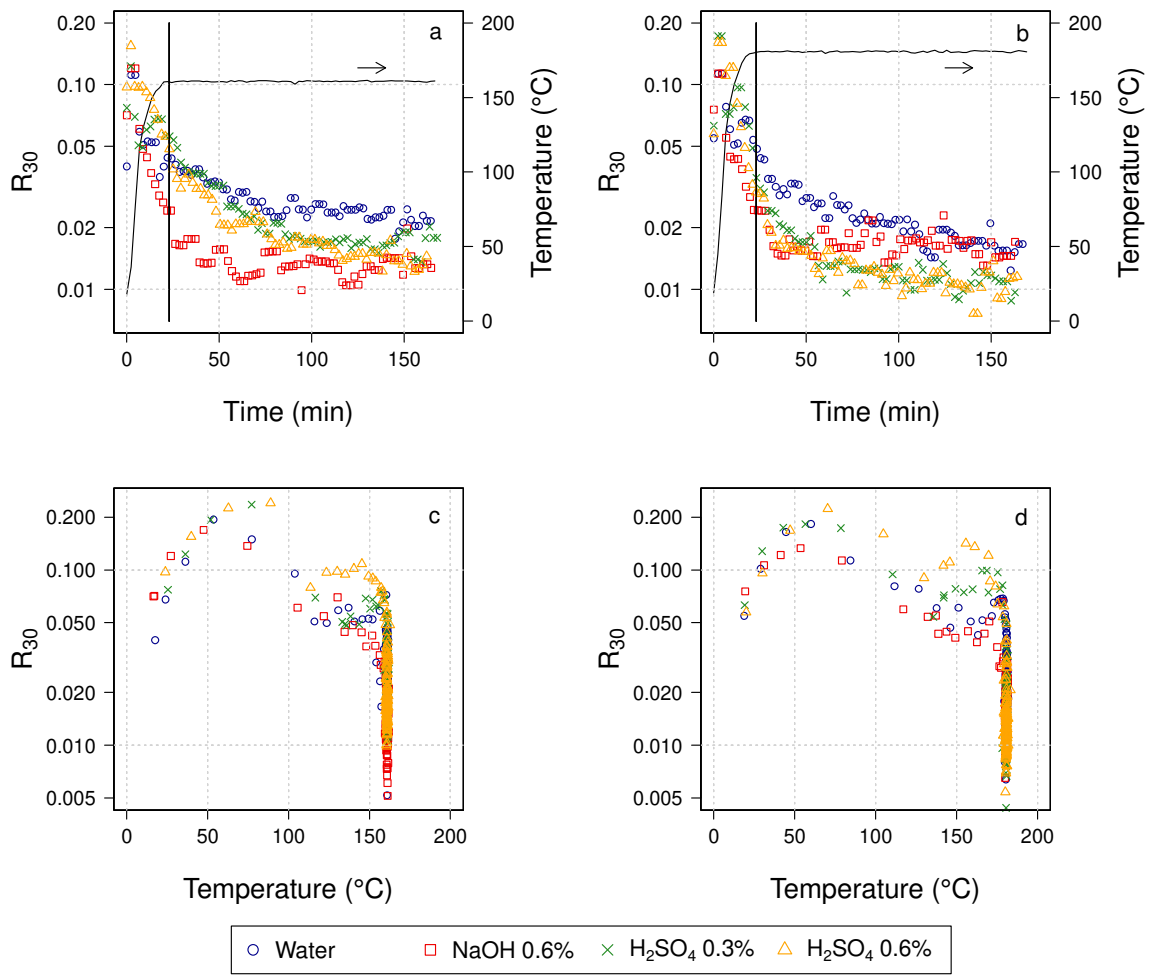
a
b
c
d
R30
Temperature (°C)
Time (min)
Temperature (°C)
Water
NaOH 0.6%
H2SO4 0.3%
H2SO4 0.6%

Figure 6:

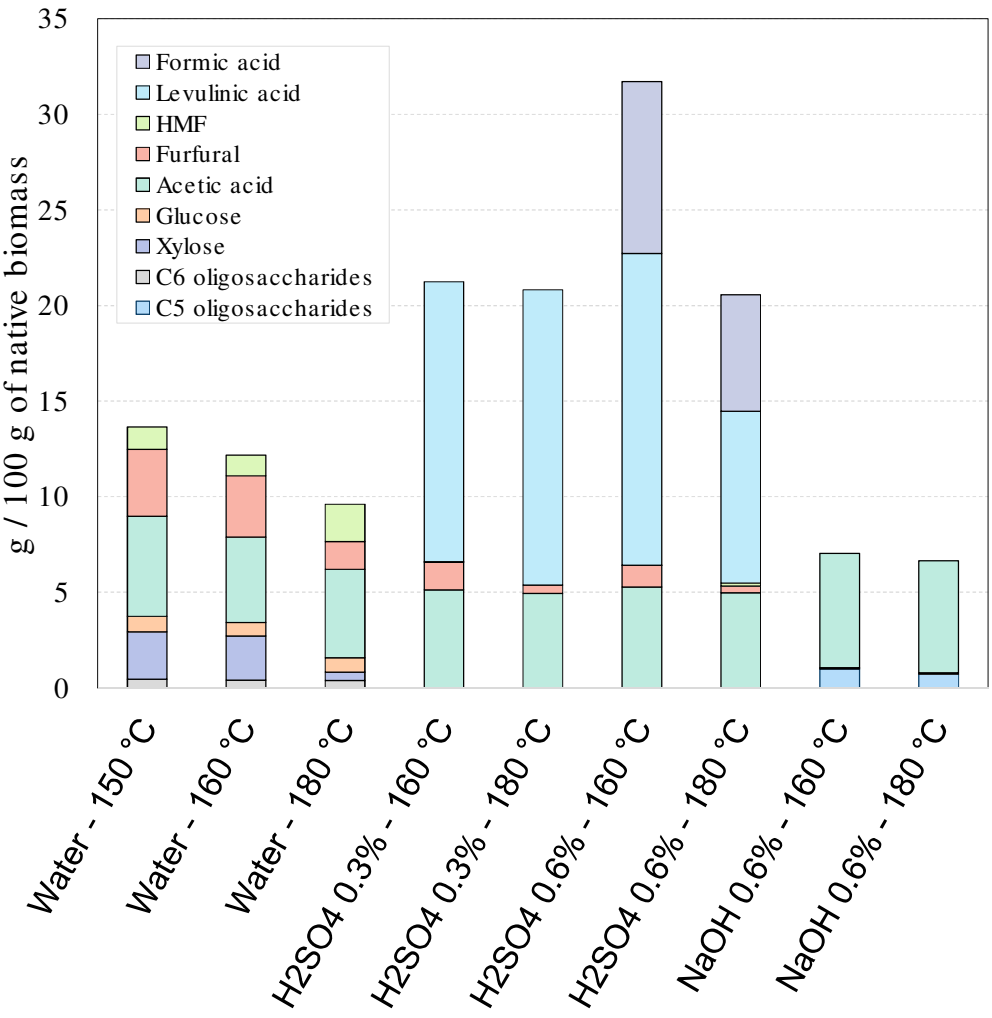
35
30
25
20
15
10
5
0
g / 100 g of native biomass
Formic acid
Levulinic acid
HMF
Furfural
Acetic acid
Glucose
Xylose
C6 oligosaccharides
C5 oligosaccharides
Water - 150 °C
Water - 160 °C
Water - 180 °C
H2SO4 0.3% - 160 °C
H2SO4 0.3% - 180 °C
H2SO4 0.6% - 160 °C
H2SO4 0.6% - 180 °C
NaOH 0.6% - 160 °C
NaOH 0.6% - 180 °C

In-line measurement of viscoelastic properties

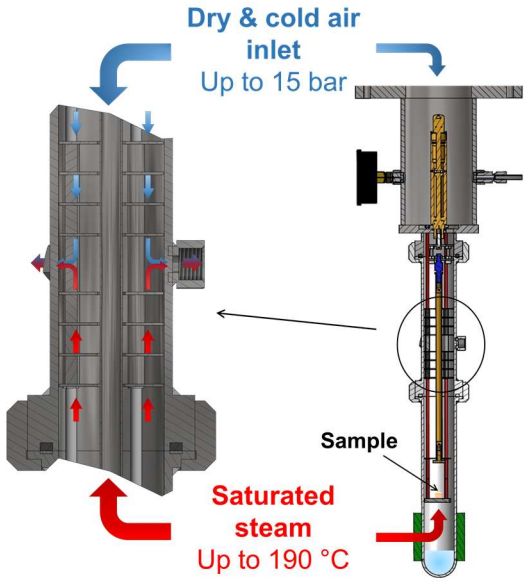

Instrumentation
T < 30 °C
RH < 50 %

Reaction chamber
RH = 100 %

Stress relaxation

Modulus of elasticity

Dynamics of chemical modifications